Nanostructure formation and cell spheroid morphogenesis of a peptide supramolecular hydrogel

Article

Accepted Version

Nanostructure Formation and Cell Spheroid Morphogenesis of a Peptide Supramolecular Hydrogel

Lucas R. Mello,[a] Vinicius Carrascosa [a], Eduardo R. L. Oliveira,[a] Maria A. Juliano,[a] Ian W. Hamley,[b] Valeria Castelletto,[b] Sandra V. Vassiliades,[c] Wendel A. Alves,[c] Clovis R. Nakaie,[a] and Emerson R. Silva[a*]

[a] Departamento de Biofísica, Universidade Federal de São Paulo, São Paulo 04023-062, Brazil;
[b] Department of Chemistry, University of Reading, Reading RGD 6AD, United Kingdom;
[c]Centro de Ciências Naturais e Humanas, Universidade Federal do ABC, Santo André 09210-580, Brazil.

ABSTRACT

Peptide-based hydrogels have attracted much attention due to their extraordinary applications in biomedicine and offer an excellent mimic for the 3D microenvironment of the extracellular matrix. These hydrated matrices comprise fibrous networks held together by a delicate balance of intermolecular forces. Here, we investigate the hydrogelation behavior of a designed decapeptide containing a tetra-leucine self-assembling backbone and fibronectin-related tripeptides near to both ends of the strand. We have observed that this synthetic peptide is able to produce hydrogel matrices entrapping > 99% wt/vol% water. Ultrastructural analysis combining atomic force microscopy (AFM), small-angle neutron scattering (SANS) and X-ray diffraction revealed that amyloid-like fibrils form crosslinked networks endowed with remarkable thermal stability, the structure of which structure is not disrupted up to temperatures > 80 °C. We also examined the interaction of peptide hydrogels with either NIH3T3 mouse fibroblasts or HeLa cells and discovered that the matrices sustain cell viability and induce morphogenesis into grape-like cell spheroids. The results presented here show that this decapeptide is a remarkable building block to prepare highly stable scaffolds simultaneously endowed with high water retention capacity and the ability to instruct cell growth into tumor-like spheroids even in non-carcinoma lineages.

*Corresponding author: er.silva@unifesp.br

INTRODUCTION

Over the last two decades, research on supramolecular hydrogels has grown exponentially because of the revolutionary applications of these materials in biomedical technology.[1–4] In addition to more conventional uses such as controlled drug release and wound dressing, hydrogels have found extraordinary applications in tissue engineering with the production of cell adhesion scaffolds, the design of artificial skin, and the 3D bioprinting of prosthetic corneas and vascularized organoids.[5–8] Indeed, the production of bioinks from peptide-based hydrogels has openned avenues for the design of organotypic cultures endowed with tunable properties.[9,10] From the perspective of basic research, these matrices are equally impressive. The 3D arrangement of the supporting medium influences a variety of cell behaviors such as proliferation, differentiation and signaling, and hydrogels are able to emulate both the topology and the chemical milieu of the extracellular matrix to provide more realistic mimics for *in vivo* conditions.[11] These remarkable features allow the culturing of multicellular spheroids that reproduce, for instance, tumoral microenvironments for cancer research[12,13] and organotypic models for drug discovery.[14]

A common strategy to produce supramolecular hydrogels is through self-assembling low molecular weight gelators (LMWG). These small molecules self-organize into nanoscopic fibers that form crosslinked or entangled networks entrapping large amounts of water through surface tension and capillary forces.[1] Short peptides have been used as efficient LMWGs for designing hydrogelled matrices able to interface with biological structures.[15] Peptides have very interesting characteristics, including biocompatibility, low immunogenicity and chemical diversity that allows the design of customized “building-blocks”. These features enable the construction of

networks with different active motifs, assisting manipulation and application of the resulting hydrogels.[16]

Herein, we investigate the hydrogelation behavior and microstructural order of a low-molecular weight peptide with the following composition: $DGRL_4DGW$ (D: aspartic acid, G: glycine, R: arginine, L: leucine and W: tryptophan). The N-terminus holds a DGR tripeptide which is the reverse sequence of the well-known fibronectin adhesion motif.[17] DGR tripeptides are part of the osteopontin cell adhesion motif and have been previously used in combination with RADA16 peptides and PEG to produce functional hydrogels.[18,19] On the other hand, the C-terminus carries a DGW tripeptide that was previously found to bind to fibronectin epitopes with high affinity.[20] We show that this designed decapeptide endowed with bolaamphiphilic characteristics can produce hydrogelled matrices entrapping > 99% wt/vol% water. Atomic force microscopy (AFM) combined with small-angle neutron scattering (SANS) revealed that supramolecular networks are formed through crosslinking of β-sheet fibers. The resulting matrices exhibit remarkable thermal stability. Although the hydrogel mesh size is found to expand as a function of temperature, likely because of a theta-to-good solvent transitions of peptide-water interactions, the structure of the hydrogel is not disrupted up to temperatures > 80 °C. We also examined the interaction of peptide hydrogels with HeLa cells and with non-carcinoma NIH3T3 mouse embryonic fibroblasts. These assays indicated that hydrogels based on $DGRL_4DGW$ peptides sustain fibroblast viability and induce cell morphogenesis into spheroid assemblies. Therefore, the results presented here show that this decapeptide is a promising building block to produce highly stable scaffolds endowed with high water retention capacity, and with an ability to induce the formation of tumor-like spheroids.

MATERIALS AND METHODS

Peptide synthesis, reagents, and sample preparation. The decameric peptide NH_2-DGRL$_4$DGW-COOH (D: aspartic acid, G: glycine, R: arginine, W: tryptophan, L: leucine) was synthesized using standard solid-phase approaches via a Fmoc strategy using Wang resin as described elsewhere.[21] Briefly, the Fmoc-Trp-Wang resin was hydrated with dichloromethane for 15 minutes and two cycles of basic hydrolysis were performed with 4-methylpiperidine in DMF (20%, 10 mL, 15 min) to remove the Fmoc protecting group. Coupling reactions were carried out with 2.50 equivalent of amino acid and 5.00 equivalent DIC and HOBt in NMP (10 mL) for 4 and 12 h (G/W/L/D and R respectively). All reaction cycles were monitored by the Kaiser ninhydrin test. The decameric peptide was deprotected and a mixture of TFA (90.0%), thioanisole (5.00%), 1,2-ethanedithiol (3.00%), and anisole (2.00%) was used to release it from the resin. The reaction was left under agitation for 4h and the supernatant was collected by vacuum filtration. Then, ice-cold diethyl ether was added to precipitate the peptide, which was successively washed with ice-cold diethyl ether and then lyophilized.[21] The yield was estimated at 40-50%. The decameric peptide was characterized by liquid chromatography coupled to mass spectroscopy (LC-MS), Figure S1, revealing that about of 86 % of the product was composed of DGWL$_4$RGD (measured Mw = 1158, calculated Mw = 1157.3). In the remaining fraction, we detected a mixture containing DGWL$_4$RGD and a product with Mw = 1140, which is associated with the release of an H_2O molecule upon spontaneous aspartimide formation between adjacent Asp and Gly side-chains.[22,23] The peptide composition and sequence were confirmed through Edman sequencing. The hydrogels were prepared through a two-step method as described elsewhere.[24] Briefly, the peptide sequence was first dissolved in cold 1,1,1,3,3,3-hexafluoro-2-isopropanol (HIFP) at a concentration of 50 mg/ml. This step was quickly

followed by the addition of ultrapure water at appropriate volumes to provide final concentrations ranging between 0.96 and 9.6 mg/ml (0.096 to 0.96 wt/vol%). To assist solubilization in water, the mixtures were submitted to ultrasonication at 40 °C for a few minutes. At this stage, the mixtures were transparent solutions, which were then transferred to an evacuated desiccator to improve the evaporation of HFIP. The formation of gels started in about 20 minutes for solutions containing ≥ 0.67 wt/vol% peptide. Samples were kept under vacuum for about 1 hour to ensure evaporation of the organic phase. Measurements of the tryptophan fluorescence were performed during the hydrogelation process of a peptide sample to assess the evaporation of HFIP from the gelled matrices. These assays indicate red shifts of tryptophan emission during the hydrogelation, which is ascribed to growth of dielectric constant of the solvent due to evaporation of HFIP (Figure S2A).[25] The tryptophan fluorescence in hydrogelled samples exhibits a maximum near to 345 nm, the same λ_{max} found in diluted samples prepared in pure water (Figure S2B), indicating that the physicochemical microenvironment in hydrogel matrices is dictated by water. Weight measurements on the resulting hydrogels indicated that the volume of organic solvent remaining in the preparations were about 4% on average.

Fluorescence assays: The fluorescence of thioflavin T (ThT) was assessed to investigate the formation of amyloidogenic aggregates. The hydrogels were prepared as described above, but instead of pure water, a 30 μM ThT solution was added in the preparation. The data were collected using a F-2500 Hitachi fluorimeter coupled to a thermostatic bath for temperature control. The excitation wavelength was kept at $\lambda_{exc.}$= 440 nm and data collection was carried out in the interval 465-650 nm, with both excitation and emission slits fixed at 10 nm. Spectra were collected immediately after addition of ThT or after a period of 90 minutes under vacuum in the desiccator to assess

fluorescence changes upon hydrogelation. Spectra from ThT solutions without peptides were used a control. Tryptophan fluorescence was also monitored to get insights into the self-assembly during hydrogelation. In this case, excitation was at $\lambda_{exc.}$= 280 nm, and 30 spectra in the 300-450 nm range were registered every 3 minutes during HFIP evaporation.

Fiber X-ray diffraction: fiber X-ray diffraction (fXRD) assays were carried out to get information on the supramolecular structure of peptide fibrils in the hydrogels. A small amount from a 0.96 wt/vol% hydrogel was suspended between the ends of wax-coated capillaries and left to dry within Petri dishes sealed with parafilm for one week at room temperature. The resulting stalks were positioned on the goniometer of a RAXIS IV++X-ray diffractometer (Rigaku) equipped with a rotating anode X-rays generator and a Saturn 992 CCD camera (pixel size 89.8 μm²). The sample-to-detector distance was 50 mm and unit-cell optimization was performed using the software CLEARER[26] to verify compatibility of the data with an orthorhombic lattice.

Circular Dichroism (CD) and Fourier transform infrared (FTIR) spectroscopy. CD spectra were measured using a JASCO-810 spectropolarimeter. Peptide hydrogels were placed in demountable Hellma cells with 0.1 mm path length, and data were collected in the range 190 – 260 nm, in steps of 1 nm and 1 s per step, using six accumulations. All data were background subtracted before further treatment, and curves were smoothed using FFT filtering (6 window points). FTIR measurements were performed on a Varian 610-IR instrument using an ATR accessory. Samples were prepared using D_2O as a solvent to avoid H_2O vibrations in the amide I range. Data were collected in the range 1575-1750 cm^{-1}, at 2 cm^{-1} resolution, using 128 accumulations. A D_2O background spectrum was subtracted from the spectra.

Microscopy assays. Hydrogels have been visualized through polarized light microscopy (PLM), electron scanning microscopy (SEM), and atomic force microscopy (AFM) to get morphology information across the mesoscopic scale. PLM experiments were performed using a Nikon Eclipse E-200 instrument equipped with cross-polarizers. A 0.96 wt/vol% hydrogel sample was sandwiched between a glass slide and a coverslip and then observed at room temperature using a 20× objective. For SEM imaging, thin layers of 0.96 wt/vol% hydrogel were cast on clean silicon substrates and left to dry overnight in a desiccator at room temperature. The samples were sputtered with a platinum film to provide a conductive layer to enable SEM imaging. Micrographs were collected using a FEI Quanta FEG 250 instrument at the center for electron microscopy of UNIFESP (CEME, UNIFESP). The microscope operated at 30 kV, with spot size at a sample of 3.0 nm and a working distance of 11.3 nm. An Everhart-Thornley detector collected secondary electrons. Typical magnifications in our experiments were between 25,000× and 150,000×. Further image treatment and enhancement were performed with ImageJ software.

AFM assays imaging was performed using a Park NX10 microscope at LNNano (CNPEM, Campinas – Brazil). Samples were prepared by casting a thin layer of gels on freshly cleaved mica substrates. The specimens were left to rest for about 5 minutes and then abundantly rinsed with ultrapure water to wash out excess gel. This procedure was carried out to obtain specimens with peptide self-assemblies adhered to mica where the sub-structures of the peptide network could be separated to allow for visualization of individual structures. The substrates were left to dry overnight in desiccators before the measurements, which were performed in tapping mode using a cantilever operating at ~75 kHz. Image visualization and enhancement were performed with software Gwyddion.

Small-angle neutron scattering (SANS). SANS experiments were carried out on the LOQ beamline at ISIS (Didicot, UK). For these assays, a 0.96 wt/vol% peptide hydrogel was prepared within a 1 mm pathlength cuvette using deuterated water (D_2O) to minimize incoherent scattering. The disc-shaped cell was accommodated in a metal rack coupled to a Julabo bath circulator to control the temperature between 25 °C and 80 °C. The acquisition time was about 40 minutes per temperature step until the detector count reached 60 μA, and the beam size at the sample was adjusted to 8 mm. A waiting time of 5 minutes was used at each temperature set point to allow for sample equilibration. The instrument operated at 25 Hz to supply neutrons with wavelengths between 2.2 Å and 10 Å, enabling access to a q-range in the interval 0.08 $nm^{-1} \leq q \leq 6$ nm^{-1}. Data fitting was performed with SASFit software, using the correlation length model proposed by Hammouda *et al.*,[27] and often used to describe nanoscale features of hydrogels:[28–30]

$$I(q) = \frac{I_0}{1 + (\xi \mathrm{q})^m} + Bkg \qquad (1)$$

In Equation (1), I_0 is the intensity at $q = 0$, and Bkg is a flat background to account for incoherent scattering. The parameter ξ is a correlation length associated with the mesh size in the case of a gel network.[31] The parameter m is a Porod exponent that also correlates with polymer-solvent interactions. For instance, $m = 2$ indicates Gaussian chains in theta conditions, whereas a $m = 5/3$ corresponds to chains in good solvent.[27]

Rheology measurements. Rheology assays were carried out as detailed elsewhere.[32] Briefly, experiments were performed using an AR-2000 rheometer (TA Instruments), using a plate-plate geometry (plate radius = 20 mm, gap = 1 mm). Measurements on both storage and loss moduli (G' and G") were carried out as a function of oscillatory stress at a fixed angular frequency of 6.283 $rad \cdot s^{-1}$ to determine the linear viscoelastic

regime, linearity being observed for $\sigma > 10$ Pa. Frequency and temperature sweeps of G' and G" were measured at $\sigma = 100$ Pa, within the linear regime.

Cell Culture and Fluorescence Imaging using Confocal Microscopy: Substrates for cell culture were prepared by placing coverslips at the bottom of 24 well plates and pouring 50 μL from a fresh 0.96 wt/vol% peptide solution on the top. The plates were left at room temperature for about 1 hour to enable evaporation of the organic solvent to trigger hydrogelation. Once hydrogelation was achieved, 1 mL of DMEM was added to the wells and left to rest for 24 hours at 37° C to infuse culture medium into the gels and wash out residual organic solvent from the matrix. After 24 hours, DMEM was washed out, and 5×10^4 NIH3T3 mouse embryonic fibroblasts or HeLa cells were seeded on the top of both hydrogel-coated and control coverslips. These cells were left to rest for 15 minutes to spread across the substrates and adhere to the surfaces. The wells were then completed with 1 mL of complete DMEM supplemented with 10% fetal bovine serum and 2 mM glutamine (Thermo Fisher Scientific). The plates with cells were kept at 37 °C in a humidified incubator under an atmosphere of 5% CO_2 for 24, 72 or 120 hours before further observations. Controls in hydrogel-free coverslips were prepared using the same protocol. After incubation, cells were washed and stained with calcein-AM to monitor the activity of esterases. After calcein staining, a fixation step was carried out by incubating the plates with 4% paraformaldehyde (PFA) for 15 minutes at room temperature. Finally, fixed cells were stained with DAPI and phalloidin (Texas red labeled) to monitor morphological changes by tracking actin distribution in the cytoskeleton. Fluorescence images were collected using a Leica TCS SP2 confocal microscope and image data treatment was carried out with LAS X softaware and Image J.

RESULTS AND DISCUSSIONS

Tube inversion assays:

The main steps for obtaining $DGRL_4DGW$ hydrogels are illustrated in Figure 1A. Samples containing peptides at final concentrations ranging from 0.096 to 0.96 wt/vol% were first assessed through tube inversion tests to determine conditions for the formation of the self-supporting gels at room temperature. These preliminary table-top assays revealed that hydrogelled matrices appear when the peptide concentration exceeds ~ 0.67 wt/vol%, a value that is interpreted as an estimation for the minimum hydrogelation concentration (MGC). The samples were kept at room temperature for several weeks, and it was verified that they have long-term stability, although samples closer to the estimated MGC exhibit signs of phase separation in 5-10 days, suggesting the release of water from the interstices of hydrogel matrix (syneresis).[33,34] Further analyses were carried out on samples prepared at 0.96 wt/vol% peptide to assure the production of stable specimens within the hydrogelation regimen. Tube inversion tests were performed to evaluate the conditions for the formation of self-supporting hydrogels upon temperature variation. In Figure 1B, photographs from a 0.96 wt/vol% peptide sample submitted to different heating conditions indicate the high stability of hydrogels across a wide range of temperatures, from 25 °C to 80 °C. Interestingly, no melting effects are observed across the temperature range, and the hydrogel matrix was found to break only at ~ 95 °C, indicating exceptionally high thermostability.

Secondary structure:

The secondary structure of hydrogels was investigated by circular dichroism (CD) and Fourier transform infrared spectroscopy (FTIR). In Figure 1C, a CD spectrum from a 0.96 wt/vol% peptide sample exhibits a very strong positive peak at 197 nm and a remarkable negative band at 219 nm. These peaks are respectively associated with $\pi \rightarrow \pi^*$ and $n \rightarrow \pi^*$ transitions in the amide chromophore N-C=O,[35] and the spectra are consistent with β-sheet conformation formed by anti-parallel aligned peptide strands.[35] In Figure 1D, the presence of an intense peak at 1627 cm^{-1} and a smaller band at 1692 cm^{-1} in the FTIR spectrum from a 0.96 wt/vol% peptide sample confirms that the secondary structure in the hydrogels is comprised of anti-parallel β-sheets.[36]

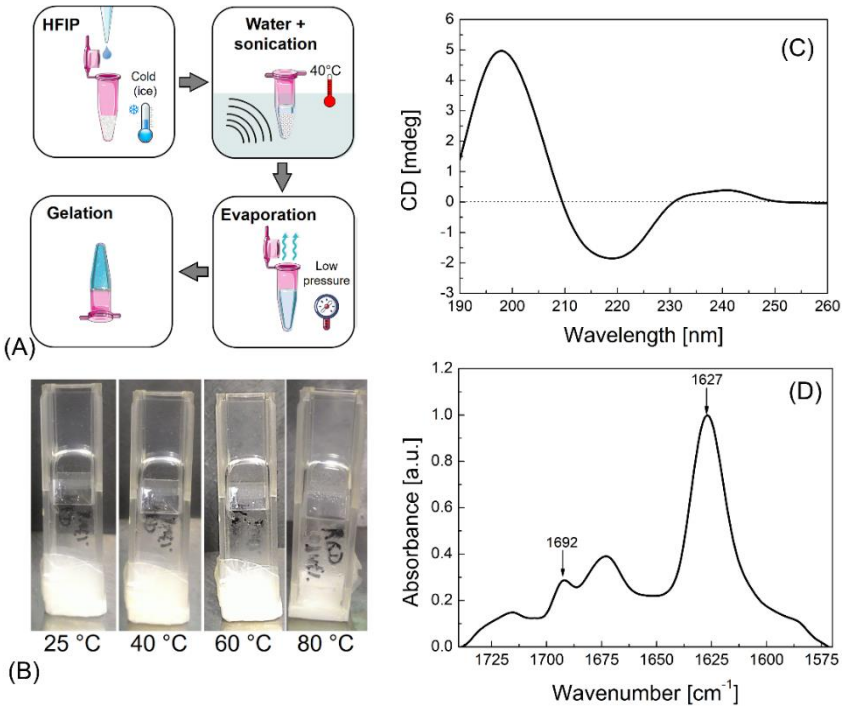

Figure 1: (A) Step-by-step representation of the hydrogelation process for $DGWL_4DRG$. (B) pictures from tube inversion tests performed on a 0.96 wt/vol% peptide sample submitted to different temperatures. (C) CD and (D) FTIR spectra from a 0.96 wt/vol% peptide hydrogel.

Microscopy imaging:

Microscopy assays were performed on hydrogel samples to unveil the morphology from the micrometer range down to the nanoscale. In Figure 2A, a PLM micrograph from a 0.96 wt/vol% peptide exhibits Schlieren textures with thread-like patterns suggesting locally-oriented domains characteristic of nematic mesophases.[37] The PLM images provide evidence for the presence of highly anisotropic assemblies in the hydrogels. We performed SEM imaging to investigate the spatial organization in greater detail. The SEM image shown in Figure 2B shows elongated structures with average thickness estimated at 99 ± 24 nm. In addition, oriented domains where fiber-like assemblies appear aligned due to excluded volume interactions between adjacent assemblies are found across the sample. At higher magnifications, inset in Fig. 2B, it is possible to discriminate finer details of these structures and identify intertwined regions.

Atomic force microscopy (AFM) was used to probe the ultrastructure of hydrogels to provide insights into morphological features of individual self-assemblies at the nanoscale. In contrast to the local tightly packed fibril aggregates observed in SEM experiments, rinsing steps carried out to prepare AFM specimens allowed the netwrk to be diluted to visualize discrete nanostructures. In Figure 2C, topography data from a 20 ×10 μm² area allows the discrimination of peptide fibrils with mean thickness 63 ± 28 nm, compatible within uncertainty with the dimensions obtained from SEM images. The AFM images also reveal fibrils entangled into larger bundles that give rise to an intricate network which is responsible for sthe elf-supporting capabilities of the hydrogel matrix. A closer inspection in Figure 2D reveals coexistence between flat and rod-like fibers. Heights of flat structures are less than 20 nm, indicating they are assembled from only a few peptide layers. In Figure 2E, an AFM image from a 1 × 1 μm² region allows visualizing fibers at a very high resolution. At this level of detail, the

topographic image shows the extensive presence of crosslinking knots between fibers responsible for holding the network together.

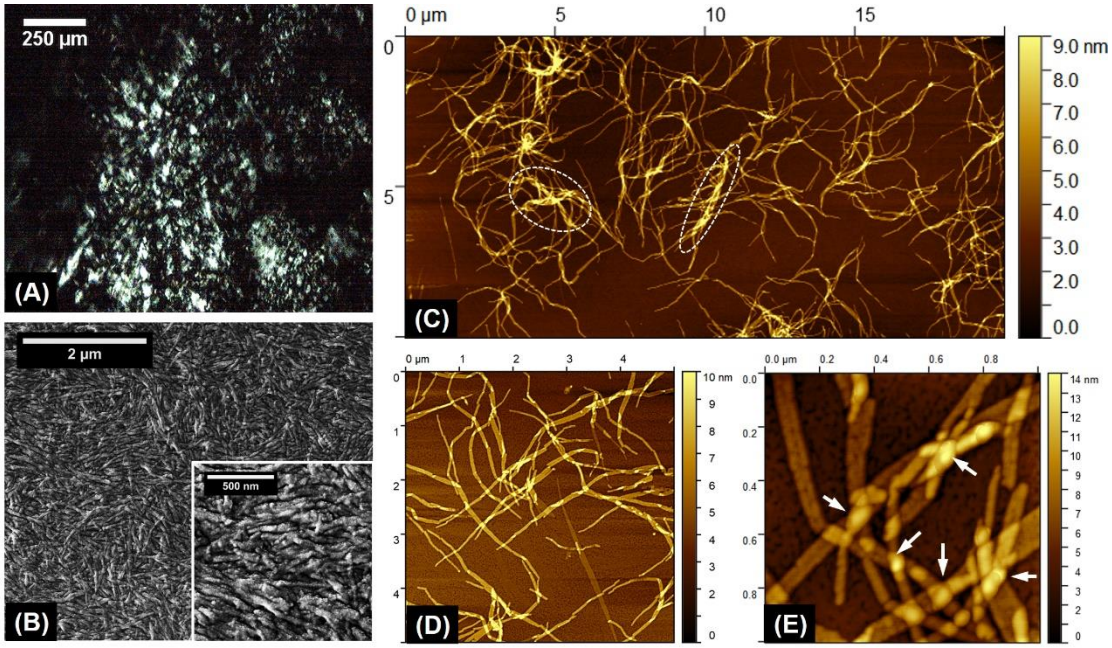

Figure 2: Microscopy images unveiling morphology features of 1wt/vol% hydrogel samples, from the micrometer range down to the nanoscale. (A) PLM image displaying Schlieren texture of nematic mesophases. (B) SEM micrograph showing an intricate network with locally oriented domains. (C) AFM topography images exhibiting discrete fibers organized into bundle-like arrangements (dashed circles). (D) Coexistence between flat and rod-like fibers. (E) Higher magnification image reveals crosslinking knots (white arrows) that stabilize the hydrogel network.

Small-angle neutron scattering:

Although the microscopy data presented above provide valuable insights into the morphology of hydrogels, such measurements were performed on dried samples which are far from native conditions. To overcome this issue, SANS was carried out to probe the mesoscale structure of the peptide network under hydrated conditions. SANS measurements were performed on a 0.96 wt/vol% peptide sample for eight temperature set points, from 25 °C to 80 °C. In Figure 3A, the double-logarithmic representation of SANS data reveals a smooth decay scaling with exponents between -1.3 and -1.7, in agreement with meshed fibrils forming mass fractal arrangements.[38–40] Subtle modifications in the shape of curves are noticed either at low q (i.e., $q < 0.2$ nm^{-1}) or at intermediate q values (1 nm^{-1} < q < 2 nm^{-1}), indicating that conformational changes appear in the hydrogel matrix upon temperature variation. Full q-range data fitting to the functional form presented in Eq (1) shows excellent agreement with the experimental data, as attested by χ^2_{red} values displayed in Table 1. In the Kratky representation shown in Figure 3B, variations between curves are emphasized and this reveals that the degree of folding of peptide fibrils decreases at higher temperatures. The Kratky plots show hyperbolic-shaped profiles, the product $I(q) \times q^2$ steeply rising with q, consistent with unfolded fibers.[41] This behavior is due to thermal fluctuations that likely appear upon heating.

Model data fitting allowed to quantify the evolution of structural parameters with temperature, as shown in Table 1. In Figure 3C, the correlation lengths (ξ) and Porod exponents (m) from the fits are plotted as a function of temperature. The parameter ξ is associated with the mesh size of the hydrogel network. Our data indicate that the dimension of pores in the matrix follow a near-constant behavior in the interval

between 25 °C and 70 °C, ranging between 7.5(3) and 9.3(4) nm, which is interpretated as evidence for thermostability. Above 70 °C, however, ξ jumps significantly to 17.7 nm, indicating expansion of the hydrogel matrix.

On the other hand, the exponent *m*, associated with polymer-solvent interactions, decreased from 1.97(2) at room temperature to 1.73(1) at 70 °C. This behavior suggests that the solvation state of the peptide network undergoes a transition from theta conditions at room temperature to good solvent conditions at higher temperatures. At 80 °C, this parameter decreases to 1.51(2), possibly due to collapse of the peptide network. The correlation length is associated with mesh size whereas the Porod exponent (*m*) is related to interactions between solvent and the fibrillar network. Since our data indicate theta-to-good solvent transitions upon temperature increase, revealing that solvation of peptide fibers become energetically more favorable, an expansion of the fibrillar network is also expected to occur. Tryptophan fluorescence has been assessed as a function of the temperature, and we found that the quantum yield decreases upon heating (Figure S2C). These findings suggest accessibility of side chains, which is consistent with theta-to-good solvent transitions in the hydrogel matrices.

As a whole, the findings derived from SANS are fully consistent with the high thermostability suggested by inversion tube tests and corroborate with rheology measurements discussed below.

Table 1. Best fitting parameters from least-square adjustment of SANS data at different temperature set points.

T [°C]	I_0 [cm^{-1}]	ξ [nm]	*m*	Bkg [cm^{-1}]	χ^2_{red}
25	3.9(2)	7.5(3)	1.97(2)	0.0269(5)	1.34
30	4.5(3)	8.5(4)	1.85(2)	0.0246(5)	0.95
37	4.7(3)	8.7(4)	1.82(2)	0.0222(4)	1.43
40	4.5(2)	7.7(3)	1.93(2)	0.0262(5)	1.05
50	5.6(2)	8.9(2)	1.85(2)	0.0254(4)	1.88
60	5.1(1)	8.6(2)	1.79(2)	0.0212(4)	2.30
70	5.3(3)	9.3(4)	1.73(1)	0.0212(2)	2.14
80	9.0(1.0)	17.7(1.7)	1.51(1)	0.0178(3)	1.71

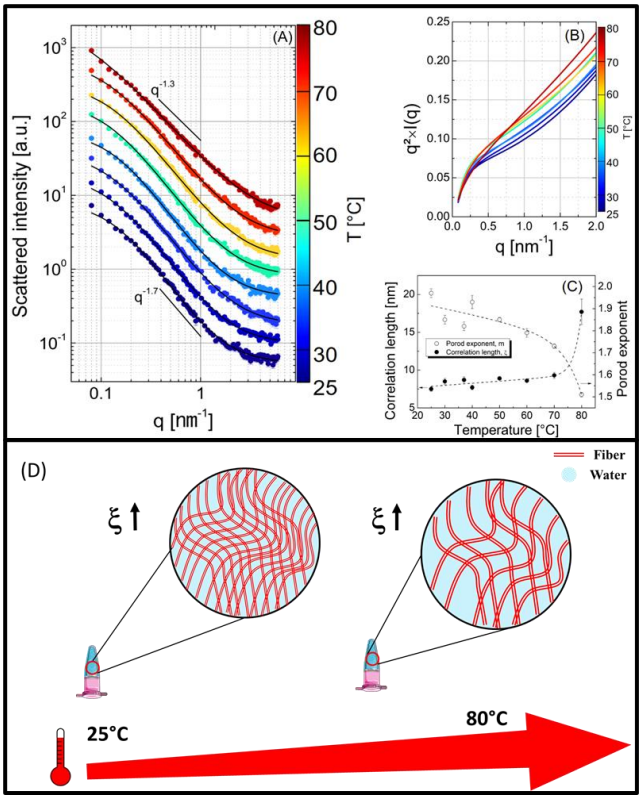

Figure 3. SANS data from a 0.96 wt/vol% peptide hydrogel, curves collected at temperature set points ranging from 25 °C to 80 °C. (A) Double-logarithmic representation of scattering profiles. Solid black lines are data fits according to the correlation length model shown in Equation (1). Curves have been shifted for clarity. (B) Kratky plots of fitted curves showing hyperbolic shapes characteristic of unfolded structures. (C) Fitted correlation lengths (ξ) and Porod exponents (*m*) as a function of temperature. Dashed lines are guides to the eye. (D) Schematic representation of the morphological changes pertaining to this network of fibers with increasing ξ upon temperature increase.

Rheology:

Rheology experiments were performed to characterize the viscoelastic properties of peptide hydrogels. Similar to SANS, these assays were carried out using hydrated samples and therefore allowed structural information to be obtained closer to native conditions. Firstly, we assessed the dependence of dynamic moduli on oscillatory stress (σ) and identified the existence of a linear regime for $\sigma > 10$ Pa (Figure S3). Then, σ was kept fixed at 100 Pa in further measurements to ensure linearity of viscoelastic properties.[42] Frequency sweeps of storage (G') and loss (G") moduli for a 0.96 wt/vol% peptide sample are shown in Figure 4A. The first feature noted is that the G' remains about one order of magnitude larger than G" across the angular frequency (ω) range. Therefore, we can conclude that the elastic component dominates the rheological reponse of these hydrogels.[43,44] A smooth increase of G' with increasing ω indicates that the gel does not have enough time to respond at high frequencies, enhancing elasticity and confirming a solid-like behavior.[45] In addition, the absence of crossover points between G' and G" indicates that hydrogels do not break in the ω range studied here. Altogether, the frequency sweep data provide clear evidence that the hydrogel structure is composed of highly crosslinked elastic networks in agreement with the morphology images shown in Figure 3.[43–45] In Figure 4B, measurements of G' and G" are presented as a function of temperature between 25 °C and 80 °C. Interestingly, the maintenance of G' > G" demonstrates that the elastic component prevails across the temperature ramp, confirming high thermostability indicated also by tube inversion tests and by SANS measurements. A slight G' decrease with increasing temperatures indicates a weakening of entanglement crosslinking upon heating, but not enough to break the hydrogel structure. The loss modulus, G", remains nearly constant across the temperature range studied. These findings correlate with SANS data, which indicated a transition from theta to good solvent condition at high temperatures.

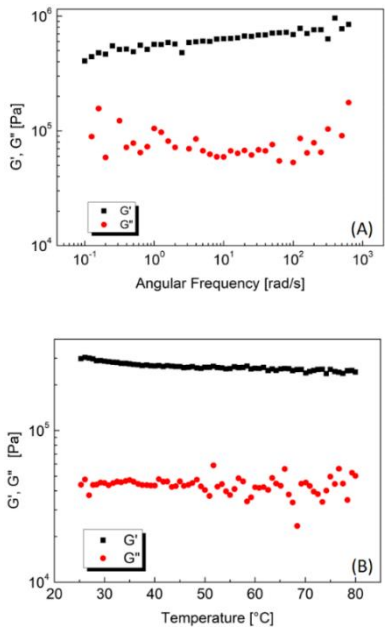

Figure 4. (A) Frequency and (B) temperature sweeps of storage (G') and loss (G") moduli for a 0.96 wt/vol% peptide hydrogel. The frequency sweep was carried out at 25 °C, whereas the temperature sweep was performed at ω = 1 rad/s.

Amyloidogenic features and hydrogelation:

We also endeavored to correlate structural information of hydrogels with the amino acid sequence to provide insight into the origin of hydrogel formation. The $DGRL_4DGW$ sequence has a triblock design as illustrated in Figure 5A, where a tetraleucine segment is flanked by more hydrophilic regions at both termini. This feature conveys a bolaamphiphilic design to the strands and favors self-assembly into tapes and fibers[46–50], nanostructures able to form hydrogel networks.[1] The presence of fibers with β-sheet conformations as indicated by FTIR and CD led us to test the hypothesis of amyloidogenic features in the gels. To get further insights into the supramolecular ordering, we monitored the fluorescence of thioflavin T (ThT) during the hydrogelation process. The yield of ThT fluorescence is known to increase upon intercalation in the grooves of pleated β-sheets found in amyloid-like fibers, thus making this dye a suitable reporter for amyloids.[51] In Figure 5B, an increase of ThT

fluorescence is observed immediately after peptide mixing (blue curve in 5B), the intensity growing by about one order of magnitude in comparison to control solutions. Upon hydrogelation, the yield increases further and reaches values 30 times higher than the control, thus suggesting that the fibers in the hydrogels possess amyloid-like features. To provide a deeper description of the supramolecular structure, we performed X-ray diffraction (XRD) on samples dried from a 0.96 wt/vol% sample. The diffractogram shown in Figure 5C is characterized by six Bragg reflections, including a very strong peak at repeat distances (*d*) of 10.8 Å, corresponding to intersheet separation between stacked β-sheets, and a reflection at *d* = 4.9 Å, consistent with interstrand spacing in anti-parallel β-sheets.[52] The set of Bragg peaks found in the diffractograms is characteristic of an orthorhombic unit cell with lattice parameters *a* = 34 Å, *b* = 11 Å, and *c* = 9.7 Å, depicted in Figure 5D. The organization into orthorhombic configuration is often found in amyloid structures.[53,54] In this configuration, $DGRL_4DGW$ strands are oriented anti-parallel, and tetraleucine cores of adjacent chains appear aligned with each other. Arginine and aspartic acid residues of neighboring strands also align with each other, and the self-assembly is likely stabilized by electrostatic attraction between oppositely charged groups in these side-chains. In addition, C-terminal tryptophans are located next to N-terminal aspartic acids and may establish ion-π interactions. Measurements carried out to probe the microenvironment of tryptophan residues during the hydrogelation process indicate fluorescence quenching (Figure S2A), consistent with ion-π interactions between tryptophan indole and aspartic acid side chains in adjacent strands.[55] Putting the findings above together, our data indicate that, except for glycine spacers, all amino acids in $DGRL_4DGW$ cooperate in the molecular self-assembly process. Moreover, this combination of leucine-driven hydrophobic effect, arginine/aspartic acid electrostatic attraction, and

tryptophan/aspartic acid íon-π interaction makes ordering into amyloid structures highly favoured. Thus, we hypothesize this high propensity to self-aggregate into amyloid fibers is on the basis of the relatively low hydrogelation concentration of $DGRL_4DGW$ and the high thermostability demonstrated by the resulting gelled matrices. With these characteristics, a small amount of peptide is sufficient to produce a high number of fibers that form dense and very cohesive networks through entanglement crosslinking of their fibril constituents (Figure 5E).

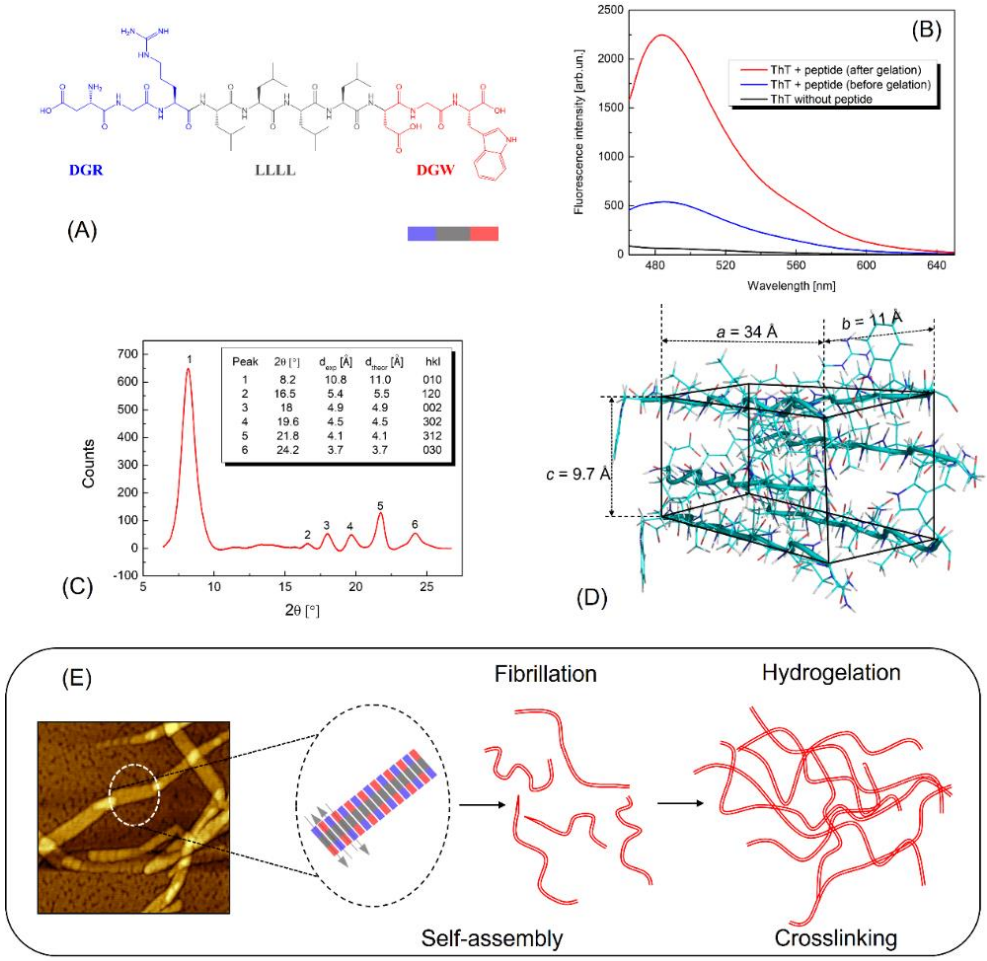

Figure 5. (A) Structure of the $DGRL_4DGW$ peptide highlighting the different blocks of amino acids. (B) Fluorescence spectra from samples containing thioflavin T showing the growth of fluorescence upon peptide self-assembly and hydrogelation. (C) X-ray diffractogram from stalks dried from a 0.96 wt% hydrogel. The inset shows both experimental and predicted peak positions along with Miller indices that are consistent

with an orthorhombic unit cell. (D) 3D model of the unit cell derived from X-ray data. (E) Schematic illustration of the anti-parallel assembly of fibrils and their entanglement crosslinking responsible for the formation of hydrogelled matrices.

Interaction with fibroblasts and carcinoma cell lines: NIH3T3 cells have been cultured on hydrogel substrates to investigate the effect of these hydrated matrices on both cytotoxicity and the topology of cellular distribution. NIH3T3 are fibroblast models widely used to investigate the interaction between cell membranes and hydrogel matrices.[56,57] In addition, these cells do not exhibit a propensity to aggregate into spheroids, thus making them suitable models for investigating this aspect in our gels. In Figure 6A, confocal fluorescence microscopy images show the morphology of the culture after 24 hours and 72 hours of incubation in the gels. In the first row, micrographs from uncoated plates display the characteristic morphology of fibroblasts with cells spreading across the surface. The cells exhibit esterase activity, as attested by calcein-AM fluorescence, indicating maintenance of viability on the surface of hydrogels.[58,59] The reddish phalloidin colour reveals the distribution of actin filaments in a 2D network linking cells to each other.[60] In contrast, cells cultured on hydrogel substrates, shown in the second row, are found assembled into spheroids where groups of cells appear aggregated. At this time point (24 h), it is possible to observe the coexistence of cells showing adhered 2D morphology along with groups of cells interacting with each other and giving raise to colonies and spheroids (see SI_video1). The calcein-AM fluorescence appears very intense, indicating strong esterase activity, thus implying that spheroids are formed from viable cells. Interestingly, the morphology of these assemblies of cells assumes the same grape-like conformations found in breast cancer cell lines used in the investigation of spheroid models.[61] The formation of spheroids is ascribed to the reorganization of the cytoskeleton and redistribution of cell-

to-surface and cell-to-cell interactions. An essential component for this process is filamentous actin (F-actin), a protein that is already linked to the self-assembly of cells in spheroid aggregates in other tissues.[62] On closer inspection, Figure 6B, the three-dimensional structure reveals that at this stage spheroids gather cells into cohesive groups with diameters of a few tens of micrometers. Reconstructions from confocal planes along the z-direction show that NIH3T3 cells stack up on top of each other, forming 3D agglomerates (see Fig. S4 and SI_video2). Figure 6C shows a 3D reconstruction of a grape-like spheroid. At this level of detail, it is possible to observe the presence of membrane projections that may anchor the assembly on the substrate. Therefore, our data suggest that $DGRL_4DGW$ hydrogels may promote cell-cell adhesive forces that induce 2D to 3D morphogenesis.[63] We hypothesize that trimeric functional groups at both ends of peptide strands play a relevant role for this cell behavior since the N-terminal DGR sequence is part of adhesion motifs in osteopontin proteins[18] and the DGW tripeptide has been reported to show affinity for fibronectin receptors.[20] In this case, these tripeptides could stimulate membrane receptors related to fibronectin fibrillization, favoring cell-cell interactions.[63–65] At 72 h, cells are still viable and are found to proliferate confirming the low cytoxocity of the gels; however, cells appear grouped into large colonies and a remarkable grape bunch morphology is observed (third row in 6A). These bunches appear to segregate and cell groups are spread across the substrate (Figs. S5-S7). At 120 h, the population of spheroids adhered to the hydrogels is reduced, indicating disengagement of these aggregates from the gels (Fig. S5 and S8). These observations indicate decrease of cell-cell interaction, similar to observations found in grape-like spheroids obtained from brest cancer cells.[61] Therefore the $DGRL_4DGW$ hydrogels are capable of inducing clear tumor-like features in non-carcinoma fibroblast cells.

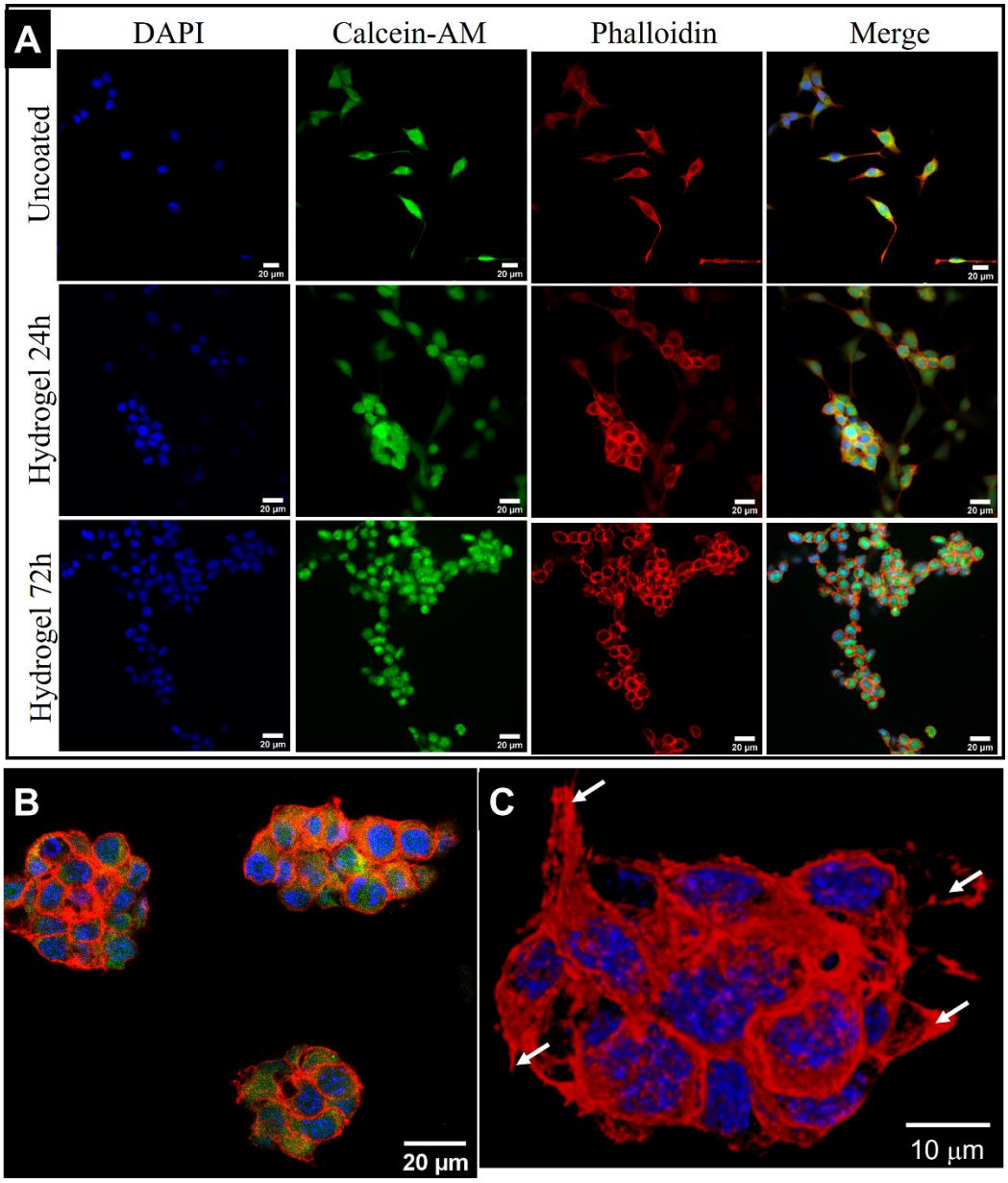

Figure 6: (A) confocal micrographs from NIH3T3 cells after 24 h and 72 h incubation: in the first row, control cells seeded on uncoated substrates exhibit the usual fibroblast 2D morphology. In the second row, cells cultured on 0.96 wt/vol% peptide hydrogels appear assembled into spheroids after 24 h. In the third row, cells cultured on hydrogel-coated surfaces proliferate into large colonies after 72 h. (B) magnified images of grape-like spheroids (24 h). (C) 3D view of a grape-like spheroid (24 h) revealing projections used to cell-cell and cell-substrate interaction.

We also investigated morphogenic effects of hydrogels on HeLa carcinoma cells. In Figure 7A and B, confocal images reveal that cells grown on the surface of hydrogels appear organized into grape-like spheroids, similar to results found in the

non-carcinoma NIH3T3 cells. Indeed, data from plates partially coated with the $DGRL_4DGW$ matrix reveal strong capacity of the peptide to induce cell-cell interactions in this lineage. Again, the successful calcein-AM staining of colonies and spheroids reveals cell viability, whereas changes in the distribution of the phalloidin fluorescence indicate reorganization of actin filaments in the cytoskeleton (Figure 7C). Cells on peptide-coated zones are observed side-by-side with their counterparts on untreated substrates, and the contrast between the 2D morphology of HeLa on uncoated surfaces and the presence of cell colonies and grape-like spheroids in the hydrogels is clear (Figure 7D). It is interesting to note that cells on either the uncoated substrate or the hydrogel surfaces shared the same culture medium; therefore, induction of spheroids is mediated by the interfaces between cell membranes and the hydrogel surface, and not by secretion signals released in the culture medium.

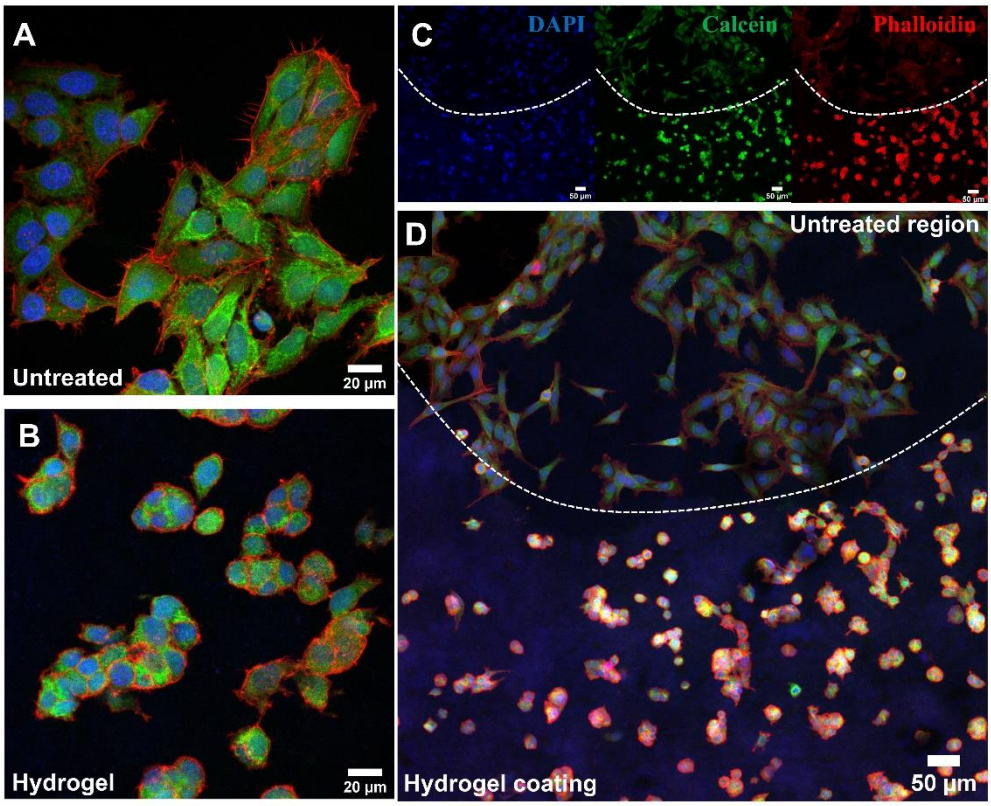

Figure 7: HeLa cells cultivated for 24 h on (A) uncoated substrates and (B) hydrogel surface. (C) and (D) Cells observed side-by-side on untreated substrates (upper) and on hydrogel-coated surfaces (bottom). The dashed line delimits the boundary between hydrogel and uncoated surfaces.

CONCLUSIONS

We have presented a detailed investigation of hydrogelation properties and assembly from the nano- to micro- scale of supramolecular hydrogels built from a self-assembling decapeptide. The peptide was designed with a triblock architecture, with a hydrophobic tetra-leucine core conjugated to fibronectin-related tripeptides at both ends of the sequence. We demonstrated that this unique design makes the peptide an efficient gelator and enables the resulting hydrogels to induce morphogenesis of tumor-like spheroids either in HeLa carcinoma cells or in non-carcinoma NIH3T3 fibroblasts. The $DGRL_4DGW$ peptide was found to form stable matrices enclosing large amounts of water at values >99% wt/vol%. Interestingly, the gels exhibit remarkable thermostability and their self-supporting capabilities are retained up to temperatures higher than 80 °C. Ultrastructural examination revealed that the matrices are composed of highly intertwined networks with amyloid-like fibrils crosslinking to form porous meshes at the nanoscale. *In situ* neutron scattering measurements indicated theta-to-good solvent transitions in the regimen of peptide-water interactions upon heating, leading to the development of peptide fibrils and the growth of pore sizes. The hydrogels were also tested regarding their interaction with NIH3T3 and HeLa cells and found to induce the formation of tumor-like assemblies, with morphogenesis into grape-like cell spheroids. These features are likely to result from the morphologenic features of $DGRL_4DGW$, since spheroid morphogenesis has been observed for NIH3T3 cells, a

fibroblast lineage which is unlikely to form tumor-like structures, as well as HeLa cells. This effect is probably a consequence of the tripeptide groups appended to the ends of the decapeptide strands, which are fibronectin epitopes. These groups likely stimulate membrane receptors that activate cell-cell interactions which in turn trigger 3D assembly. The matrices are able to sustain cell viability and grape-like spheroids produced from fibroblasts remain stable for periods of at least 72 h, similar to observations found in spheroids produced with breast cell lines.[61] In summary, the results presented here demonstrate that this type of triblock peptide design may be suitable for designing peptide gelators to produce highly stable matrices endowed with cell modulation capabilities.

SUPPORTING INFORMATION

HPLC-MS data, tryptophan fluorescence, rheology characterization, additional cell imaging, SI_video1: z-scan from NIH3T3 spheroid, SI_video2: z-scan from adhered NIH3T3 cells morphing into spheroid, SI_vide3: z-scan from HeLa spheroids.

ACKNOWLEDGEMENTS

This work has been primarily supported by the Sao Paulo Research Foundation (FAPESP) through a Regular Grant to ERS (#2019/200907-7) and PhD fellowships to LRM (#2019/19719-1 and #2021/10092-6). ERS is a fellow of the Brazilian Research Council (# 310916/2019-4). Vinícius Carrascosa acknowledges the internal program for scientific initiation (PIBIC-UNIFESP) for an undergraduate fellowship. We are grateful

to the National Nanotechnology Laboratory (LNNano) for awarding shifts for AFM measurements (# AFM-27464), and Dr. Carlos Costa is kindly acknowledged for assistance during AFM data collection. SANS experiments were carried out on beamline LOQ at ISIS (proposal 1810004), and we thank James Doutch for assistance. We acknowledge Prof. Sang W. Han for granting access to facilities for cell culture experiments. IWH and VC acknowledge EPSRC (UK) for funding from Platform grant ref. EP/L020599/1. We also thank Elizabeth Naomi for help during data collection on the Leica SP8 confocal instrument (FAPESP project n° 09/52430-3 granted to Prof. Helena B. Nader) at the multiuser platform of INFAR-UNIFESP. W.A.A acknowledges CNPq (grant n◦ 304389/2019-6), the National Institute of Science and Technology in Bioanalytics (FAPESP grant no. 2014/50867-3 and CNPq grant no. 465389/2014-7), and FAPESP (grant no. 2017/02317-2). CN acknowledges FAPESP (grant n° 18/23269-9).

REFERENCES

(1) Draper, E. R.; Adams, D. J. Low-Molecular-Weight Gels: The State of the Art. *Chem* **2017**, *3* (3), 390–410.

(2) Das, S.; Das, D. Rational Design of Peptide-Based Smart Hydrogels for Therapeutic Applications. *Front. Chem.* **2021**, *9*.

(3) Fu, K.; Wu, H.; Su, Z. Self-Assembling Peptide-Based Hydrogels: Fabrication, Properties, and Applications. *Biotechnol. Adv.* **2021**, *49*, 107752.

(4) Fosgerau, K.; Hoffmann, T. Peptide Therapeutics: Current Status and Future Directions. *Drug Discov. Today* **2015**, *20* (1), 122–128.

(5) Dey, M.; Ozbolat, I. T. 3D Bioprinting of Cells, Tissues and Organs. *Sci. Rep.* **2020**, *10* (1), 14023.

(6) Isaacson, A.; Swioklo, S.; Connon, C. J. 3D Bioprinting of a Corneal Stroma Equivalent. *Exp. Eye Res.* **2018**, *173*, 188–193.

(7) Gouveia, R. M.; Castelletto, V.; Hamley, I. W.; Connon, C. J. New Self-Assembling Multifunctional Templates for the Biofabrication and Controlled Self-Release of Cultured Tissue. *Tissue Eng. Part A* **2015**, *21* (11–12), 1772–1784.

(8) Zhang, Y.; Kumar, P.; Lv, S.; Xiong, D.; Zhao, H.; Cai, Z.; Zhao, X. Recent Advances in 3D Bioprinting of Vascularized Tissues. *Mater. Des.* **2021**, *199*, 109398.

(9) Jian, H.; Wang, M.; Dong, Q.; Li, J.; Wang, A.; Li, X.; Ren, P.; Bai, S. Dipeptide Self-Assembled Hydrogels with Tunable Mechanical Properties and Degradability for 3D Bioprinting. *ACS Appl. Mater. Interfaces* **2019**, *11* (50), 46419–46426.

(10) Loo, Y.; Lakshmanan, A.; Ni, M.; Toh, L. L.; Wang, S.; Hauser, C. A. E. Peptide Bioink: Self-Assembling Nanofibrous Scaffolds for Three-Dimensional Organotypic Cultures. *Nano Lett.* **2015**, *15* (10), 6919–6925.

(11) Tibbitt, M. W.; Anseth, K. S. Hydrogels as Extracellular Matrix Mimics for 3D Cell Culture. *Biotechnol. Bioeng.* **2009**, *103* (4), 655–663.

(12) Li, Y.; Kumacheva, E. Hydrogel Microenvironments for Cancer Spheroid Growth and Drug Screening. *Sci. Adv.* **2018**, *4* (4), eaas8998.

(13) Worthington, P.; Pochan, D. J.; Langhans, S. A. Peptide Hydrogels – Versatile Matrices for 3D Cell Culture in Cancer Medicine. *Front. Oncol.* **2015**, *5*, 92.

(14) Liu, H.; Wang, Y.; Cui, K.; Guo, Y.; Zhang, X.; Qin, J. Advances in Hydrogels in Organoids and Organs-on-a-Chip. *Adv. Mater.* **2019**, *31* (50), 1902042.

(15) Chen, L.; Morris, K.; Laybourn, A.; Elias, D.; Hicks, M. R.; Rodger, A.; Serpell, L.; Adams, D. J. Self-Assembly Mechanism for a Naphthalene-Dipeptide Leading to Hydrogelation. *Langmuir* **2010**, *26* (7), 5232–5242.

(16) Radvar, E.; Azevedo, H. S. Supramolecular Peptide / Polymer Hybrid Hydrogels for Biomedical Applications. *Macromol. Biosci.* **2018**, *19* (1), 1–16.

(17) Gouveia, R. M.; Castelletto, V.; Alcock, S. G.; Hamley, I. W.; Connon, C. J. Bioactive Films Produced from Self-Assembling Peptide Amphiphiles as Versatile Substrates for Tuning Cell Adhesion and Tissue Architecture in Serum-Free Conditions. *J. Mater.*

Chem. B **2013**, *1* (44), 6157–6169.

(18) Horii, A.; Wang, X.; Gelain, F.; Zhang, S. Biological Designer Self-Assembling Peptide Nanofiber Scaffolds Significantly Enhance Osteoblast Proliferation, Differentiation and 3-D Migration. *PLoS One* **2007**, *2* (2), 1–9.

(19) Castelletto, V.; Gouveia, R. J.; Connon, C. J.; Hamley, I. W. Self-Assembly and Bioactivity of a Polymer/Peptide Conjugate Containing the RGD Cell Adhesion Motif and PEG. *Eur. Polym. J.* **2013**, *49* (10), 2961–2967.

(20) Pasqualini, R.; Koivunen, E.; Ruoslahti, E. A Peptide Isolated from Phage Display Libraries Is a Structural and Functional Mimic of an RGD-Binding Site on Integrins. *J. Cell Biol.* **1995**, *130* (5), 1189–1196.

(21) Decandio, C. C.; Vassiliades, S. V.; Gerbelli, B. B.; Aguilar, A. M.; Alves, W. A. Hybrid Hydrogels Based on Polyethylene Glycol Bioconjugated with Silylated-Amyloidogenic Peptides. *J. Braz. Chem. Soc.* **2020**.

(22) Mergler, M.; Dick, F.; Sax, B.; Weiler, P.; Vorherr, T. The Aspartimide Problem in Fmoc-Based SPPS. Part I. *J. Pept. Sci.* **2003**, *9* (1), 36–46.

(23) Lauer, J. L.; Fields, C. G.; Fields, G. B. Sequence Dependence of Aspartimide Formation during 9-Fluorenylmethoxycarbonyl Solid-Phase Peptide Synthesis. *Lett. Pept. Sci.* **1995**, *1* (4), 197–205.

(24) Souza, S. F.; Kogikoski, S.; Silva, E. R.; Alves, W. A. Nanostructured Antigen-Responsive Hydrogels Based on Peptides for Leishmaniasis Detection. *J. Braz. Chem. Soc.* **2017**, *28* (9).

(25) Vivian, J. T.; Callis, P. R. Mechanisms of Tryptophan Fluorescence Shifts in Proteins. *Biophys. J. 80* (5), 2093–2109.

(26) Makin, O. S.; Sikorski, P.; Serpell, L. C. CLEARER: A New Tool for the Analysis of X-Ray Fibre Diffraction Patterns and Diffraction Simulation from Atomic Structural Models. *J. Appl. Crystallogr.* **2007**, *40*, 966–972.

(27) Hammouda, B.; Ho, D. L.; Kline, S. Insight into Clustering in Poly(Ethylene Oxide) Solutions. *Macromolecules* **2004**, *37* (18), 6932–6937.

(28) Hammouda, B. Clustering in Polar Media. *J. Chem. Phys.* **2010**, *133* (8), 84901.

(29) Hule, R. A.; Nagarkar, R. P.; Hammouda, B.; Schneider, J. P.; Pochan, D. J. Dependence of Self-Assembled Peptide Hydrogel Network Structure on Local Fibril Nanostructure. *Macromolecules* **2009**, *42* (18), 7137–7145.

(30) Hule, R. A.; Nagarkar, R. P.; Altunbas, A.; Ramay, H. R.; Branco, M. C.; Schneider, J. P.; Pochan, D. J. Correlations between Structure, Material Properties and Bioproperties in Self-Assembled Beta-Hairpin Peptide Hydrogels. *Faraday Discuss* **2008**, *139*, 225-251,419-420.

(31) Saffer, E. M.; Lackey, M. A.; Griffin, D. M.; Kishore, S.; Tew, G. N.; Bhatia, S. R. SANS Study of Highly Resilient Poly(Ethylene Glycol) Hydrogels. *Soft Matter* **2014**, *10* (12), 1905–1916.

(32) Castelletto, V.; Hamley, I. W. Amyloid and Hydrogel Formation of a Peptide Sequence from a Coronavirus Spike Protein. *ACS Nano* **2022**.

(33) Panja, S.; Dietrich, B.; Adams, D. J. Controlling Syneresis of Hydrogels Using Organic

Salts. *Angew. Chemie Int. Ed.* **2022**, *61* (4), e202115021.

(34) Castilla, A. M.; Wallace, M.; Mears, L. L. E.; Draper, E. R.; Doutch, J.; Rogers, S.; Adams, D. J. On the Syneresis of an OPV Functionalised Dipeptide Hydrogel. *Soft Matter* **2016**, *12* (37), 7848–7854.

(35) Rogers, D. M.; Jasim, S. B.; Dyer, N. T.; Auvray, F.; Réfrégiers, M.; Hirst, J. D. Electronic Circular Dichroism Spectroscopy of Proteins. *Chem* **2019**, *5* (11), 2751–2774.

(36) Barth, A. Infrared Spectroscopy of Proteins. *Biochim. Biophys. Acta - Bioenerg.* **2007**, *1767* (9), 1073–1101.

(37) Davies, R. P. W.; Aggeli, A.; Beevers, A. J.; Boden, N.; Carrick, L. M.; Fishwick, C. W. G.; Mcleish, T. C. B.; Nyrkova, I.; Semenov, A. N. Self-Assembling β-Sheet Tape Forming Peptides. *Supramol. Chem.* **2006**, *18* (5), 435–443.

(38) Pedersen, J. S. Analysis of Small-Angle Scattering Data from Colloids and Polymer Solutions: Modeling and Least-Squares Fitting. *Adv. Colloid Interface Sci.* **1997**, *70* (0), 171–210.

(39) Clover, B.; Hammouda, B. SANS from P85/Water-d under Pressure. *Langmuir* **2010**, *26* (9), 6625–6629.

(40) Hamley, I. W. *Small-Angle Scattering: Theory, Instrumentation, Data and Applications*, 1st ed.; Wiley: Chichester, 2021.

(41) Rambo, R. P.; Tainer, J. A. Characterizing Flexible and Intrinsically Unstructured Biological Macromolecules by SAS Using the Porod-Debye Law. *Biopolymers* **2011**, *95* (8), 559–571.

(42) Hamley, I. W.; Kirkham, S.; Dehsorkhi, A.; Castelletto, V.; Reza, M.; Ruokolainen, J. Toll-like Receptor Agonist Lipopeptides Self-Assemble into Distinct Nanostructures. *Chem. Commun.* **2014**, *50* (100), 15948–15951.

(43) Mousavi, S. M. R.; Rafe, A.; Yeganehzad, S. Structure-Rheology Relationships of Composite Gels: Alginate and Basil Seed Gum/Guar Gum. *Carbohydr. Polym.* **2020**, *232*, 115809.

(44) Liu, Y.; Winter, H. H.; Perry, S. L. Linear Viscoelasticity of Complex Coacervates. *Adv. Colloid Interface Sci.* **2017**, *239*, 46–60.

(45) Ghobril, C.; Grinstaff, M. W. The Chemistry and Engineering of Polymeric Hydrogel Adhesives for Wound Closure: A Tutorial. *Chem. Soc. Rev.* **2015**, *44* (7), 1820–1835.

(46) da Silva, E. R.; Walter, M. N. M.; Reza, M.; Castelletto, V.; Ruokolainen, J.; Connon, C. J.; Alves, W. A.; Hamley, I. W. Self-Assembled Arginine-Capped Peptide Bolaamphiphile Nanosheets for Cell Culture and Controlled Wettability Surfaces. *Biomacromolecules* **2015**, *16* (10), 3180–3190.

(47) da Silva, E. R.; Alves, W. A.; Castelletto, V.; Reza, M.; Ruokolainen, J.; Hussain, R.; Hamley, I. W. Self-Assembly Pathway of Peptide Nanotubes Formed by a Glutamatic Acid-Based Bolaamphiphile. *Chem. Commun.* **2015**, *51* (58), 11634–11637.

(48) Hamley, I. W.; Burholt, S.; Hutchinson, J.; Castelletto, V.; da Silva, E. R.; Alves, W.; Gutfreund, P.; Porcar, L.; Dattani, R.; Hermida-Merino, D.; Newby, G.; Reza, M.; Ruokolainen, J.; Stasiak, J. Shear Alignment of Bola-Amphiphilic Arginine-Coated Peptide Nanotubes. *Biomacromolecules* **2017**, *18* (1), 141–149.

(49) Mello, L. R.; Aguiar, R. B.; Yamada, R. Y.; Moraes, J. Z.; Hamley, I. W.; Alves, W. A.; Reza, M.; Ruokolainen, J.; Silva, E. R. Amphipathic Design Dictates Self-Assembly, Cytotoxicity and Cell Uptake of Arginine-Rich Surfactant-like Peptides. *J. Mater. Chem. B* **2020**, *8* (12), 2495–2507.

(50) Mello, L. R.; Hamley, I. W.; Castelletto, V.; Garcia, B. B. M.; Lourenço, T. C.; Vassiliades, S. V; Alves, W. A.; Han, S. W.; Silva, E. R. Self-Assembly and Intracellular Delivery of DNA by a Truncated Fragment Derived from the Trojan Peptide Penetratin. *Soft Matter* **2020**, *16* (20), 4746–4755.

(51) Nilsson, M. R. Techniques to Study Amyloid Fibril Formation in Vitro. *Methods* **2004**, *34* (1), 151–160.

(52) Decandio, C. C.; Silva, E. R.; Hamley, I. W.; Castelletto, V.; Liberato, M. S.; Oliveira, V. X.; Oliveira, C. L. P. P.; Alves, W. A. Self-Assembly of a Designed Alternating Arginine/Phenylalanine Oligopeptide. *Langmuir* **2015**, *31* (15), 4513–4523.

(53) Mello, L. R.; Hamley, I. W.; Miranda, A.; Alves, W. A.; Silva, E. R. β-Sheet Assembly in Amyloidogenic Glutamic Acid Nanostructures: Insights from X-Ray Scattering and Infrared Nanospectroscopy. *J. Pept. Sci.* **2019**, *25* (6), e3170.

(54) Jahn, T. R.; Makin, O. S.; Morris, K. L.; Marshall, K. E.; Tian, P.; Sikorski, P.; Serpell, L. C. The Common Architecture of Cross-Beta Amyloid. *J. Mol. Biol.* **2010**, *395* (4), 717–727.

(55) Lakowicz, J. R. *Principles of Fluorescence Spectroscopy* , 4th ed.; Springer: New York, 2006.

(56) Wang, Y. Q.; Zhang, Z. L.; Xu, L.; Li, X. Y.; Chen, H. Hydrogels of Halogenated Fmoc-Short Peptides for Potential Application in Tissue Engineering. *Colloids and Surfaces B-Biointerfaces* **2013**, *104*, 163–168.

(57) Kretsinger, J. K.; Haines, L. A.; Ozbas, B.; Pochan, D. J.; Schneider, J. P. Cytocompatibility of Self-Assembled β-Hairpin Peptide Hydrogel Surfaces. *Biomaterials* **2005**, *26* (25), 5177–5186.

(58) White, K.; Chalaby, R.; Lowe, G.; Berlin, J.; Glackin, C.; Olabisi, R. Calcein Binding to Assess Mineralization in Hydrogel Microspheres. *Polymers (Basel).* **2021**, *13* (14), 2274.

(59) Koh, W.-G.; Pishko, M. V. Fabrication of Cell-Containing Hydrogel Microstructures inside Microfluidic Devices That Can Be Used as Cell-Based Biosensors. *Anal. Bioanal. Chem.* **2006**, *385* (8), 1389–1397.

(60) Mazloom-Farsibaf, H.; Farzam, F.; Fazel, M.; Wester, M. J.; Meddens, M. B. M.; Lidke, K. A. Comparing Lifeact and Phalloidin for Superresolution Imaging of Actin in Fixed Cells. *PLoS One* **2021**, *16* (1 January), 1–13.

(61) Kenny, P. A.; Lee, G. Y.; Myers, C. A.; Neve, R. M.; Semeiks, J. R.; Spellman, P. T.; Lorenz, K.; Lee, E. H.; Barcellos-Hoff, M. H.; Petersen, O. W.; Gray, J. W.; Bissell, M. J. The Morphologies of Breast Cancer Cell Lines in Three-Dimensional Assays Correlate with Their Profiles of Gene Expression. *Mol. Oncol.* **2007**, *1* (1), 84–96.

(62) Tzanakakis, E. S.; Hansen, L. K.; Hu, W.-S. The Role of Actin Filaments and Microtubules in Hepatocyte Spheroid Self-Assembly. *Cell Motil.* **2001**, *48* (3), 175–189.

(63) Wang, H.; Feng, Z.; Xu, B. Intercellular Instructed-Assembly Mimics Protein Dynamics To Induce Cell Spheroids. *J. Am. Chem. Soc.* **2019**, *141* (18), 7271–7274.

(64) Wolanska, K. I.; Morgan, M. R. Fibronectin Remodelling: Cell-Mediated Regulation of the Microenvironment. *Biochem. Soc. Trans.* **2015**, *43* (1), 122–128.

(65) Mao, Y.; Schwarzbauer, J. E. Fibronectin Fibrillogenesis, a Cell-Mediated Matrix Assembly Process. *Matrix Biol.* **2005**, *24* (6), 389–399.

GRAPHICAL ABSTRACT